

# A Harmonic Compensation Strategy for Grid-connected Inverter with LCL Filter

Xiaowei Dong, Yize Sun\*, Yujie Chen, Jie Yang

College of Mechanical Engineering, Donghua University  
No. 2999, North Renmin Road, Shanghai, China, 201620

\*Corresponding author, e-mail: sunyz@dhu.edu.cn

## Abstract

LCL filter has the characteristic of prompt attenuation over the high-frequency range, but the third-order control system exits the resonance problem. Nonetheless, the inherent non-linear characteristic and dead-time effects of switching tubes, along with the DC-side voltage secondary pulsation and grid harmonic pollution, arouse a wealth of low-order harmonics injected which is tough to be filtered. In this paper, a combined control scheme of repetitive control and state feedback is brought forward, in which both DC voltage feedforward and grid voltage feedforward are added. The proposed control strategy can eliminate resonance peak of LCL filter, suppress and compensate the low-frequency harmonics, so that quick response and tracking without static error of the system can be realized. Finally, the rationality of the harmonic analysis and the validity of control strategy are verified through MATLAB simulation and experiment results of the grid-connected inverter.

**Keywords:** grid-connected inverter, LCL filter, harmonic, state feedback, repetitive control

**Copyright © 2014 Institute of Advanced Engineering and Science. All rights reserved.**

## 1. Introduction

Grid-connected inverter, as the interface between the distributed generation power and the grid, is widely used in photovoltaic, wind and other renewable energy power generation systems. Both the harmonic suppression capability and the quality of grid-connected current waveform are important performance indicators of the grid-connected inverter [1, 2].

The DC power come from the renewable power generation units can be transformed into pulse voltage which changes in the rules of sine wave after modulation of switching tubes in the inverter circuit. The modulation of the switching tubes, however, could bring in the harmonics of switching frequency and the higher-frequency. Meanwhile the filtering element leads to transition process and instability of the system, thus it's crucial that the addition of the suitable regulator to assure the steady-state and dynamic performance of the system [3, 4]. The high-frequency harmonics resulted from the modulation would be easy to be eliminated by the filter. While the low-frequency harmonics that are difficult to be filtered, as a result of non-ideal situations and external disturbances, will seriously influence the output voltage and the grid-tied current. The current controller, thus, needs further optimization to offset the low-order harmonic pollution, but few literatures associated with the overall analysis and quantitative calculations of the low-frequency harmonics can be found.

Since the velocity of amplitude attenuation over high-frequency range is -60dB/decade, the LCL filter has an advantage of better attenuation characteristics for higher-frequency harmonics over the pure-inductance filter. Nevertheless, for third-order control model, there is one high resonance peak at the resonance frequency, which will give rise to the distortion of current waveform. Therefore, the appropriate control strategy should be taken advantage of to improve the system damping so as to enhance the stability of the system [5, 6]. The traditional passive damping scheme inserting a resistor in serials or parallel into the filter, result in the corresponding damping loss together with weakening the ability to attenuate the high-frequency harmonics, which is unsatisfactory. While the typical active damping technology includes the split capacitor method, the inner-loop feedback of capacitor current method, the deadbeat control method, and so forth [7-9]. The gain of conventional PI regulator at alternating component is  $|K_p + K_i / j\omega_0|$ , so there is steady-state error. By contrast, infinite gain at some

specific frequency can be generated when adopting the PR control and the repetitive control, which pose excellent suppression of the periodic disturbances, so that the tracking without static error could be achieved [10-12].

In this paper, the model of a single-phase grid-connected inverter with LCL filter is established. Then, it's quantitatively analyzed that the impact of inherent non-linear characteristics and dead-time effects of switching tubes, the impact of DC voltage secondary pulsation and grid harmonics on the grid-tied current, under the unipolar double-frequency sinusoidal pulse-width modulation (SPWM). Furthermore, a combined control scheme of embedded repetitive control and state feedback is brought forward, in which DC voltage feedforward decoupling and the grid voltage feedforward compensation are added. Finally, the rationality of the harmonic analysis and the validity of the combined control scheme presented in this article are verified on the 3kW inverter system.

## 2. System Model of the Single-phase Grid-connected Inverter with LCL-filter

Table 1. Parameters of grid-tied connected LCL inverter

Symbol	Description	Value
$P$	Rated output power	3kW
$u_{dc}$	DC bus voltage	420V
$u_s$	PCC voltage(RMS)	220V
$f_0$	Grid frequency	50Hz
$C_{dc}$	DC stabilized capacitor	2000uF
$f_c$	Switch frequency	16kHz
$f_s$	Sample frequency	32kHz
$T_d$	Dead-time	3μs
$L_1$	Inverter-side inductance	3mH
$R_1$	$L_1$ parasitic resistance	0.5Ω
$L_2$	Grid-side inductance	0.6mH
$R_2$	$L_2$ parasitic resistance	0.1Ω
$C_f$	Filter capacitor	4.7μF
$P$	Rated output power	3kW

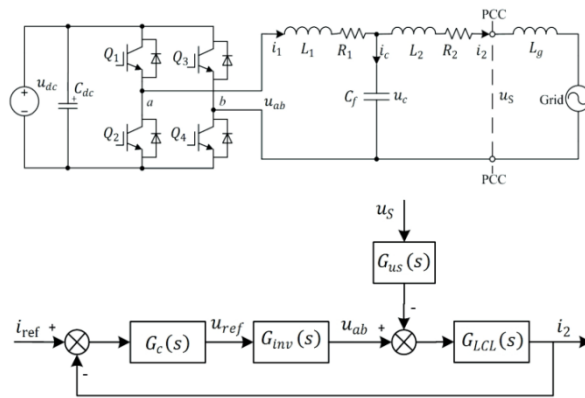


Figure 1. Topology and Control Diagram of Single-phase Grid-connected Inverter with LCL Filter

In order to analyze the mathematic model of the LCL filter, it is selected  $x = [i_1, i_2, u_c]^T$  as the state variable,  $y = [i_2]$  as the output variable,  $u = [u_{ab}, u_s]^T$  as the system input and disturbance, thus the system state-space equation can be established as follow:

$$\begin{cases} \dot{x} = Ax + Bu \\ y = Cx \end{cases} \quad (1)$$

Where:

$$A = \begin{bmatrix} -\frac{R_1}{L_1} & 0 & -\frac{1}{L_1} \\ 0 & -\frac{R_2}{L_2} & \frac{1}{L_2} \\ \frac{1}{C_f} & -\frac{1}{C_f} & 0 \end{bmatrix}, B = [B_1 \quad B_2] = \begin{bmatrix} \frac{1}{L_1} & 0 \\ 0 & -\frac{1}{L_2} \\ 0 & 0 \end{bmatrix}, C = [0 \quad 1 \quad 0] \quad (2)$$

Figure 1 illustrates the topology and control diagram of the single-phase grid-connected inverter with LCL filter whose parameters are listed in Table 1. The object of the current loop controller is a dual-input/single-output system.  $i_{ref}$  is the instruction current signal, which can be calculated by the previous maximum power point tracking unit, or determined by the grid-power. Then  $i_{ref}$  is compared with the feedback signal of grid-connected current  $i_2$ , and the result

signal is sent to the current controller  $G_c(s)$ . The Point of Common Couple voltage (PCC)  $u_s$  can be seen as disturbance signal, whose forward path transfer function is  $G_{us}(s)$ .

### 3. Harmonic Analysis for Grid-connected Inverter

#### 3.1. Unipolar Double-frequency SPWM Technology

As the most widely applied modulation method in the single-phase inverter system, SPWM has advantages of fixed switching frequency and facilitation of digital implementation. Under the unipolar double-frequency modulation, the output voltage ripple frequency is as twice as switching frequency and harmonics are greatly reduced, which is of benefit to filtering.

The drive signal of switching tubes  $Q_1$  and  $Q_2$  could be obtained by comparison of  $u_r$  with the carrier wave  $u_c$ , while the drive signal of  $Q_3$  and  $Q_4$  could be achieved by comparison of  $u_r$  with the reverse carrier wave  $-u_c$ .

In Figure 2, the equations of the modulation wave and the carrier wave can be set as follows:

$$u_r = U_m \sin(\omega_0 t + \varphi) \quad (3)$$

$$u_c = \begin{cases} -(\omega_c t - 2\pi k - 2\pi) \frac{2U_{cm}}{\pi} - U_{cm}, & 2\pi k + \pi \leq \omega_c t \leq 2\pi k + 2\pi \\ (\omega_c t - 2\pi k) \frac{2U_{cm}}{\pi} - U_{cm}, & 2\pi k \leq \omega_c t \leq 2\pi k + \pi \end{cases} \quad (4)$$

The PWM waves are generated by comparison of  $u_r$  with  $u_c$  and  $-u_c$ , respectively. It can be easy to get the mathematical expression of the output voltage  $u_{ab}$ . After conducting the double Fourier series expansion, the following equation could be attained:

$$u_{ab}(t) = MU_{dc} \sin(\omega_0 t + \varphi) + \frac{2U_{dc}}{\pi} \sum_{m=1,2,\dots}^{\infty} \sum_{n=\pm 1, \pm 3, \dots}^{\pm \infty} (-1)^m \frac{J_n(mM\pi)}{m} \sin(2m\omega_c t + n\omega_0 t + n\varphi) \quad (5)$$

Where  $M$  denotes modulation degree, which can be calculated by  $M = U_m / U_{cm}$  ( $U_m$  and  $U_{cm}$  are the amplitude of the modulation wave and carrier wave, respectively), and generally  $U_{cm} = 1$ ;  $\omega_0$  serves as the angular frequency of modulation wave;  $\omega_c$  is the angular frequency of the carrier wave;  $J_n(x)$  refers to the Bessel function.

#### 3.2. The Injection of the Low-order Harmonics under Internal Non-ideal Situation

It is necessary to add dead-time into the drive signal to avoid switching tubes of the same phase leg opening simultaneously. The dead-time effects together with the inherent non-linear of switching devices can lead to the loss of the fundamental voltage, the distortion of the output current, and the injection of the low-order harmonics. The actual output voltage wave of single leg during one switching period is displayed in Figure 3. As for  $i_1 > 0$ , the current flows through the power tube  $T_1$ , and  $U_{a0} = U_{dc} / 2$  over the range of  $T_{on}$ ; while through the diode  $D_2$ , and  $U_{a0} = -U_{dc} / 2$  over the range of  $T_{off}$ . As for  $i_1 < 0$ , the current flows through the power tube  $T_2$  and  $U_{a0} = -U_{dc} / 2$  over the range of  $T_{off}$ ; while through the diode  $D_1$ , and  $U_{a0} = U_{dc} / 2$  over the range of  $T_{on}$ .

In Figure 3,  $T_s$  is the switching period;  $T_{on}$  is the opening interval;  $T_{off}$  is the shutdown interval;  $T_{dead}$  is the dead time;  $t_{on}$  is the on-time of the switching tube;  $t_{off}$  is the off-time of the switching tube;  $T_d$  is the equivalent error time;  $V_D$  is the conduction voltage drop of diode;  $V_T$  is the conductive voltage drop of power tube;  $V_{drop}$  is the overall voltage drop of switching tube;  $U_{a0}$  is the ideal output voltage of the single leg;  $U'_{a0}$  is the output voltage considering dead time;

$U''_{a0}$  is the output voltage considering the switching turned-on and turned-off time;  $V_{a0}$  is the actual output voltage considering the conductive voltage drop;  $\Delta V_{d0}$  is the mean error voltage and can be calculated by  $\Delta V_{d0} = V_{a0} - U_{a0}$ .

According to the above analysis, the expression of the mean error voltage  $\Delta V_{d0}$  by the equivalent area method of high-frequency pulse can be derived as Equation (6):

$$\begin{cases} \Delta V_{d0} = -\frac{T_d}{T_s} U_{dc} \text{sign}(i_1) \\ T_d = T_{dead} + t_{on} - t_{off} + \frac{V_{drop}}{U_{dc}} T_s \\ V_{drop} = \begin{cases} \frac{T_{on}}{T_s} V_T + \frac{T_{off}}{T_s} V_D, i_1 > 0 \\ \frac{T_{off}}{T_s} V_T + \frac{T_{on}}{T_s} V_D, i_1 < 0 \end{cases} \end{cases} \quad (6)$$

The error voltage between the two legs of the single-phase inverter is doubled, i.e.  $\Delta v_d = 2\Delta v_{d0}$ . After Fourier series expansion is implemented, following equation can be obtained:

$$\Delta v_d = -\frac{8U_{dc}T_d}{k\pi T_s} \cos k\omega_0 \frac{T_z}{2} \sum_{k=1,3,\dots}^{\infty} \sin[k(\omega_0 t)] \quad (7)$$

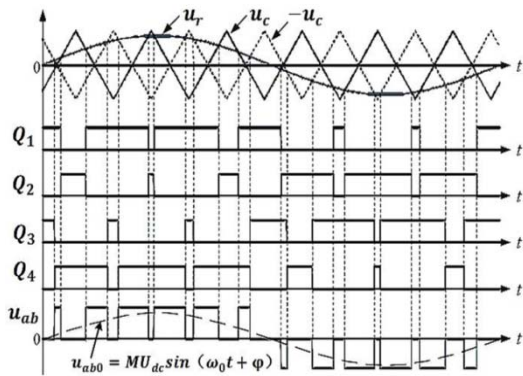


Figure 2. Principle of Unipolar Double-frequency SPWM

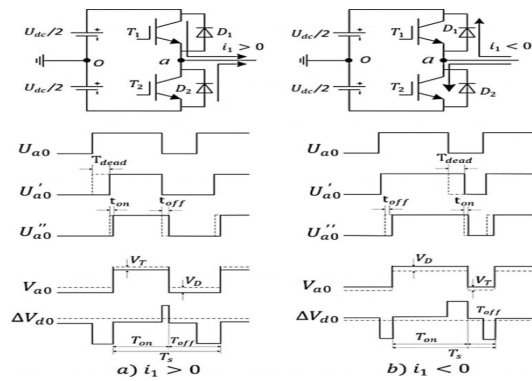


Figure 3. Ideal Versus Actual Output Voltage Waveform of the Leg

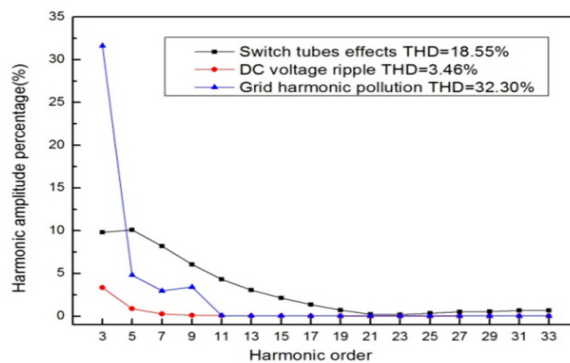


Figure 4. Low-order Harmonic Distribution of the Grid-tied Current under Different Disturbances

Generally, the turned-off time  $t_{off}$  is longer than the turned-on time  $t_{on}$ . Thus, to some extent, the dead-time effects resulted from the dead time  $T_{dead}$  would be weakened. The conductive voltage drop  $V_{drop}$ , however, would strengthen the dead-time effects. The mean error voltage  $\Delta V_{d0}$  is characteristic of the periodical square wave, whose amplitude is constant and polarity is opposite to the polarity of inductance current. Taking the inductance current ripple into consideration, there is a considerable wide range of the zero-crossing sector  $T_z$ . Due to the positive and negative offset, the amplitude of  $\Delta V_{d0}$  is zero, thus dead-time effects disappear in the  $T_z$ .

Under the conditions of constant dead time and zero-crossing sector, the amplitude of the error voltage is related to the DC-side voltage, the switching cycle, and the harmonic frequency. What's more, the first component could result in the loss of the fundamental wave of the inverter bridge output voltage and the output current distortion. While the odd number components of the triple or above could inject the low-order harmonics, leading to the decline in the wave quality of output voltage and grid-connected current.

### 3.3. The Injection of Low-order Harmonics Caused by External Disturbances

The external disturbances of inverter system mainly come from DC-side voltage fluctuations and the grid voltage harmonic pollution. There is usually secondary pulsation among the DC-side voltage, whose root cause is the instantaneous imbalance between the AC power and the DC power. Assuming that the grid-connected inverter is unity power factor running, there is the component whose frequency is as twice as the grid fundamental frequency in the inverter instantaneous output power, apart from the stable DC component. The secondary pulsation  $\Delta u_{dc}$  must be provided by the electrolytic capacitor in the DC side, as illustrated by the following equations:

$$P = I_m U_m \sin^2(\omega_0 t) = \frac{I_m U_m}{2} [1 - \cos(2\omega_0 t)] \quad (8)$$

$$\begin{cases} \Delta u_{dc} = \varepsilon U_{dc} \cos(2\omega_0 t) \\ \Delta u_{ab}(t) = M \Delta u_{dc} \sin(\omega_0 t + \varphi) = \frac{M \varepsilon U_{dc}}{2} [\sin(3\omega_0 t + \varphi) - \sin(\omega_0 t - \varphi)] \end{cases} \quad (9)$$

Wherein  $\varepsilon$  is the voltage ripple coefficient.

There is intermodulation between the modulated fundamental component and the secondary pulsation component of DC voltage, thus the first and the triple components are included in the actual output voltage of the inverter bridge. If it could not be suppressed by the current controller, the triple component would be multiplied by  $\Delta u_{dc}$  circularly and repeatedly, hence the other odd-order harmonic components would be generated in the grid-connected current.

The voltage drop on the equivalent grid impedance arising out of the harmonic current caused by the non-linear loads, together with the saturation of the transmission and distribution transformers can all contribute to the distortion of the grid voltage. Furthermore, the harmonic components are added into the grid voltage, which mainly include odd-order harmonics, such as triple, five-order, seven-order, and so forth. Consequently, the output current also contains low-order harmonics at the corresponding frequency.

### 3.4. Harmonic Analysis of Grid-connected Current

The LCL-filter inverter differs from the pure-inductance in the attenuation speed only over the high-frequency range, while they both have the identical amplitude-frequency characteristic over the low-frequency range. Therefore, it will be adequate representation and simplified calculation taking the L-filter inverter to analyze the low-order harmonics. Ignoring the inductance parasitic resistance and setting  $L_T = L_1 + L_2$ , the grid fundamental current  $i_{L0}$  and the low-order harmonic current  $i_{Ln}$  can be expressed as the following two equations, respectively.

$$i_{L0} = \frac{u_{ab0} + \Delta v_{d0} + \Delta u_{ab0} - u_{s0}}{L_T j\omega_0} = \frac{MU_{dc} - \frac{8U_{dc}T_d}{\pi T_s} \cos k\omega_0 \frac{T_z}{2} - \frac{M\epsilon U_{dc}}{2} - U_s}{L_T j\omega_0} \tag{10}$$

$$i_{Ln} = \sum_{k=3,5,7,\dots} \frac{\Delta v_{dn}}{L_T k j\omega_0} + \sum_{p=3,5,7,\dots} \frac{\Delta u_{abn}}{L_T p j\omega_0} - \sum_{q=2,3,4,\dots} \frac{u_{sn}}{L_T q j\omega_0} \quad (n = 2,3,4,\dots) \tag{11}$$

The fundamental component loss of the grid-tied current can be equivalent to the damping loss of the inductance branch, and it should be compensated in the design of the system power. The high-frequency harmonics of the inverter output voltage can easily attenuated through the filter, thus there are scarcely high-order components in the grid-connected current. It is necessary to add the feedback compensation part or the high-impedance harmonic suppressor at some specific frequency into the current controller to eliminate the low-frequency harmonics that mainly include odd-order components. Figure 4 exhibits the low-order harmonic distribution of grid-connected current under different disturbances.

#### 4. Harmonic Compensation Strategy for Grid-tied Inverter

It is brought forward that a combined control scheme of repetitive control and state feedback, in which the feedforward decoupling for DC voltage and the feedforward compensation for grid voltage are added, as shown in Figure 5.

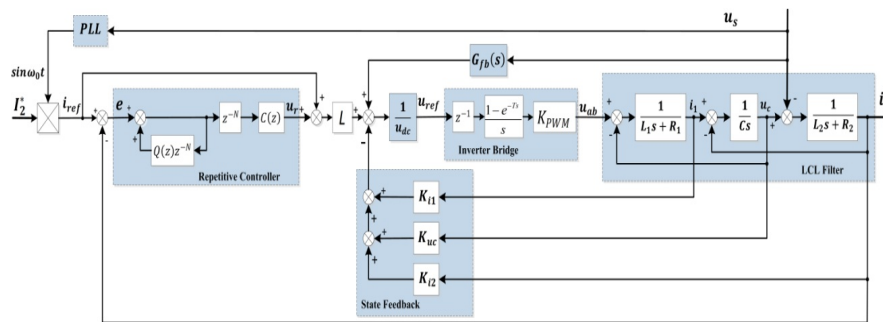


Figure 5. Block Diagram of Current Control Scheme

#### 4.1. The Pole Assignment of State Feedback

The reason of the poor dynamic performance of the grid-tied inverter with LCL-filter is that the damping of the system itself is too weak, i.e. one pair of conjugate poles and one real pole are too closed to the imaginary axis in the S plane. The most direct and effective resolution is to insert state feedback to place the poles of closed-loop system in the desirable position by means of selecting appropriate feedback gain matrix [13]. The grid-connected inverter with LCL filter is a third-order system. The grid voltage  $u_s$  is taken as the disturbance, and then it would be conducted that pole assignment of the system input  $u_{ab}$ , i.e. to set two conjugate dominant poles, while to place another real pole quite far away from the imaginary axis, as shown in Equation (12):

$$\begin{cases} s_{1,2} = -\xi_r \omega_r \pm j\sqrt{1-\xi_r^2} \omega_r \\ s_3 = -m\xi_r \omega_r \end{cases} \tag{12}$$

Wherein  $\xi_r, \omega_r$  are the expected damping ratio and natural frequency, respectively. The greater the value of  $m$  is, the closer the response characteristic of third-order system is to the second-order system determined by two closed-loop conjugate dominant poles, and  $m = 4 \sim 10$ , generally.  $\omega_r$  should be slightly smaller than the resonance frequency of the LCL filter

calculated by  $\omega = \sqrt{(L_1 + L_2) / L_1 L_2 C_f}$ , and there is also additive damping in the actual system.  $\xi_r = 0.5, \omega_r = 20000, m = 4$  are adopted in this paper based on the above analyses.

As shown in Equation (13), The gain matrix can be obtained by applying pole assignment calculation method.

$$K = \begin{bmatrix} K_{i1} \\ K_{i2} \\ K_{uc} \end{bmatrix} = \begin{bmatrix} 179 \\ -45.32 \\ 10.78 \end{bmatrix} \quad (13)$$

After pole assignment, the transfer functions of the input and the disturbance versus the output are shown in Equation (14), (15), respectively.

$$G_1(s) = C(A - KB_1)^{-1} B_1 \quad (14)$$

$$G_2(s) = C(A - KB_1)^{-1} B_2 \quad (15)$$

In order to make the step response tracking error of the system input equal to zero, the forward path gain can be calculated as below:

$$\begin{cases} e_{ss} = \lim_{s \rightarrow \infty} s \left( \frac{1}{s} - \frac{LG_1(s)}{s} \right) = 0 \\ L = K_{i1} + K_{i2} + K_{uc} R_2 + R_1 + R_2 = 135.36 \end{cases} \quad (16)$$

#### 4.2. Design of DC and Grid Voltage Feedforward

Directly from the modulation principle in this paper, the modulation degree  $M$  is set as a variable factor with respect to  $u_{dc}$ , and then the carrier wave or the modulation wave would be reconstructed. The transfer function of the inverter bridge  $G_{inv}(s)$  could be normalized through the voltage feedforward decoupling in order to keep the system gain stable and eliminate the harmonic components caused by the DC voltage fluctuations, which is expressed in Equation (17).

$$u_{ab} = \frac{u_r}{u_{dc}} K_{PWM} = \frac{u_r}{u_{dc}} \frac{u_{dc}}{U_{cm}} = u_r * 1 \quad (17)$$

The grid voltage disturbance can be compensated by the feedforward path  $G_{fb}(s)$ , which can be calculated by the following equations.

$$G_{us}(s) - G_{fb}(s)G_{inv}(s) = 0 \quad (18)$$

$$G_{fb}(s) = \frac{G_{us}(s)}{G_{inv}(s)} = C_f L_1 s^2 + C_f (K_{i1} + R_1) s + K_{uc} + 1 \quad (19)$$

Since the noise is easy to be amplified in the differentiation element, and dual-differentiation is complex to realize through software method. Therefore the partial feedforward is adopted in this paper, whose coefficient is determined by  $G_{fb}(s) = K_{uc} + 1 = 11.78$ .

#### 4.3. Design of Repetitive Controller

The repetitive controller is based on internal model principle. According to the error of the former fundamental cycle, the correction signal can be attained. Then it will be superimposed on the original control signal at the same time of the latter fundamental cycle so as to eliminate the repetitive distortion that would show up during all the next fundamental

periods, and further to achieve tracking without no static error [14]. It can be found in Fig. 5 that the repetitive internal model  $G(z)$  is composed of two parts (integral and delay), as restated in Equation (20).

$$G(z) = \frac{z^{-N}}{1 - Q(z)z^{-N}} \tag{20}$$

Where  $Q(z) = 0.95$  is adopted and  $N$  refers to sampling number during one fundamental cycle. The gain  $K_r$  of the compensator as depicted in Equation (21) generally is  $0 \sim 1$ . The phase of the entire system can be compensated by the anticipatory element  $z^k$ , so that the phase error over the low-frequency range is zero. As resonance peaks have been eliminated by the pole assignment, it's unnecessary to set the trap filter. As a result,  $S(z)$  should be set as two-order low-pass filter to enhance the high-frequency attenuation.

$$C(z) = K_r z^k S(z) = 1 * z^k * Z \left( \frac{\omega_n^2}{s^2 + 2\xi\omega_n s + \omega_n^2} \right) \tag{21}$$

The rapid response performance of system is gravely affected by the period delay part  $z^{-N}$ . The delay part  $z^{-N}$  has tremendous control lag, whence the prompt path of the instruction signal should be retained by using the embedded structure.  $P(z)$  is the discrete transfer function of the controlled object, and  $d(z)$  is the system disturbance, thus the relationship between the error and the instruction as well as the disturbance is revealed in Equation [22].

$$e = i_{ref} - (i_{ref} + u_r) * P - d = \frac{(1-P)(1-Qz^{-N})}{1-z^{-N}(Q-CP)} i_{ref} - \frac{1-Qz^{-N}}{1-z^{-N}(Q-CP)} d \tag{22}$$

The error caused by the disturbance can be attenuated to  $\left| \frac{1-Q}{1-(Q-CP)} \right|$ , thus the closer  $Q(z)$  is to 1, the smaller the error is. While arbitrary order harmonics can be wiped off by the ideal repetitive controller when  $Q(z) = 1$ .

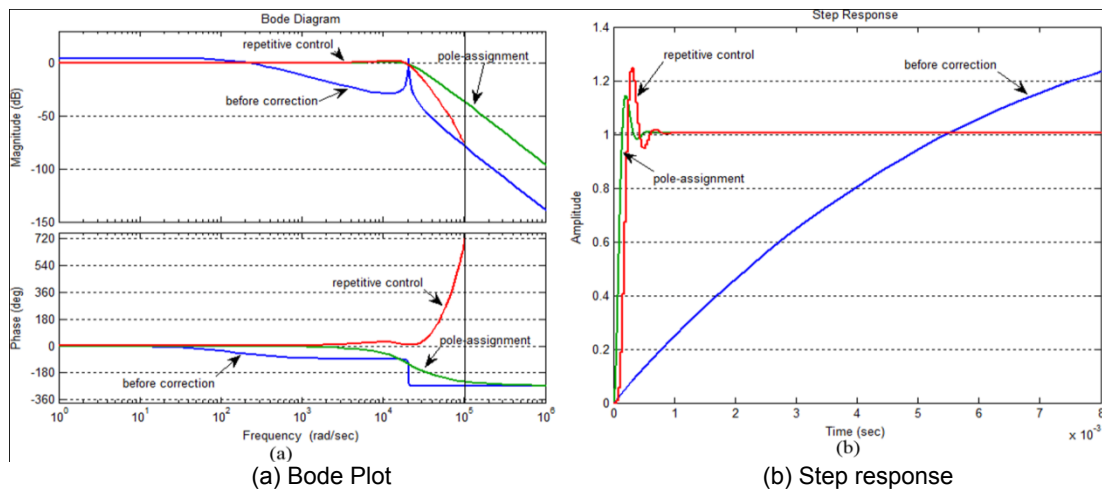


Figure 6. Characteristics of Grid-connected Current Before Versus After Correction

As shown in Figure 6, the LCL-filter has relatively poor open-loop characteristic, enormously high resonance peak as well as amplitude and phase distortion over the middle-frequency range. By contrast, after pole assignment, the system resonance peak is eliminated, with zero gain and zero phase-shift over middle-frequency range. The ideal dynamic response

speed and excellent stability are achieved when tracing the grid-connect instruction. After repetitive control compensator is inserted, the ability of the high-frequency attenuation can be further strengthened by  $S(z)$ . Meanwhile, the system phase lag can be compensated by the anticipatory part  $z^k$ . The phase anticipatory over the high-frequency range couldn't make any effect upon the system because the high-order noise is effectively damped. The repetitive internal model can effectively suppress the low-order harmonics injected by periodical disturbances, such as dead-time effects and grid voltage. Meanwhile the steady-state error over the fundamental frequency range is eliminated.

## 5. Simulation and Experiment

The simulation experiment is conducted under different control strategies which consist of without the current correction, the state feedback adopted solely, and the combined control scheme. As listed in Table 2, the state feedback method can damp harmonic components. However, it still couldn't meet the requirements of the international PV system grid-connected standard, i.e. IEEE Std.929-2000 [15]. Nevertheless, the harmonic components can perfectly satisfy the grid-connected requirements after using the combined control scheme.

Table 2. Comparison of Low-order Harmonics under Different Control Schemes

Harmonic Distortions (%)	3 <sup>rd</sup> – 9 <sup>th</sup>	11 <sup>st</sup> – 15 <sup>th</sup>	17 <sup>th</sup> – 21 <sup>st</sup>	23 <sup>rd</sup> – 33 <sup>rd</sup>	≥ 33 <sup>rd</sup>	THD
Dead-time and Disturbance	46.49	18.10	7.10	4.81	9.03	51.42
State Feedback	10.40	0.52	0.39	0.30	0.33	10.53
Repetitive Control and Feedforward	0.07	0.03	0.02	0.02	0.07	0.12
IEEE Std.929-2000	<4	<2	<1.5	<0.6	<0.3	<5

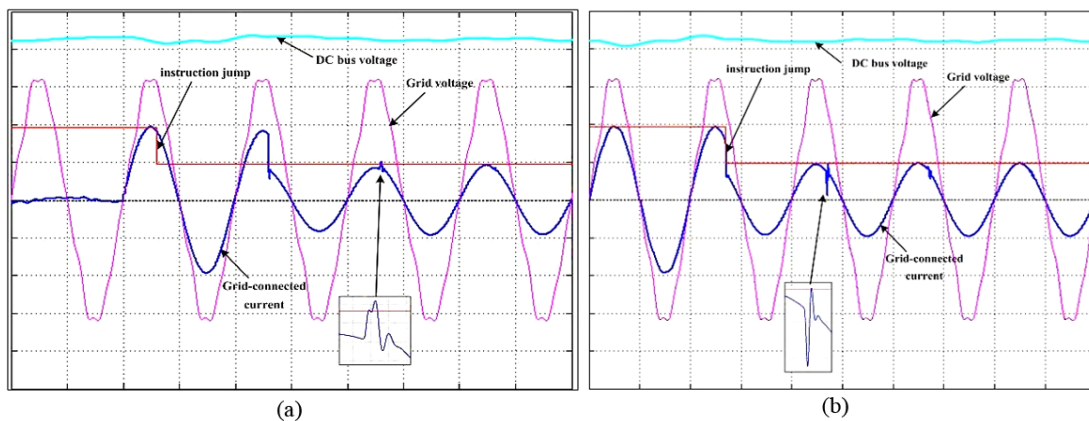


Figure 7. Simulation Waveforms when Instruction Jump Happens under Different Repetitive Controller (u:100V/div, i:10A/div, t:10ms/div)

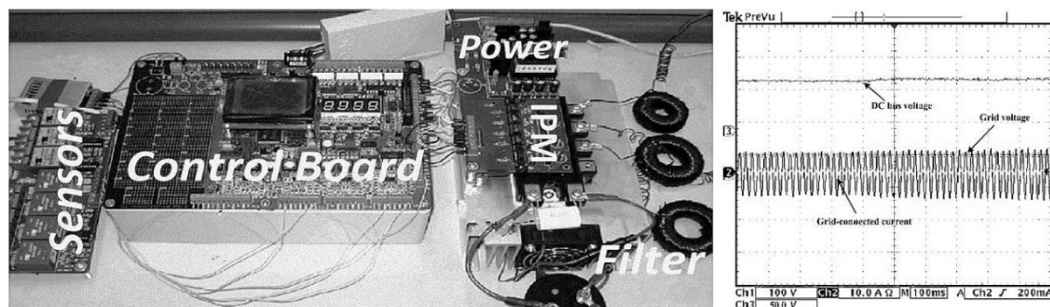


Figure 8. Experimental Devices and Steady-state Waveforms

The wave form of the instruction current when the load changes from full-load to half-load is illustrated in Figure 7. The response to the instruction change has a fundamental cycle delay when the repetitive controller is connected in series as shown in Figure 7(a); while as shown in Figure 7(b), for the embedded repetitive control method, because the rapid response path of the instruction is added, the instruction current can be traced by the grid-tied current promptly when sudden changes happen. What's more, the accumulative distortion effects resulted from the instantaneous current error can be substantially eliminated after two cycles.

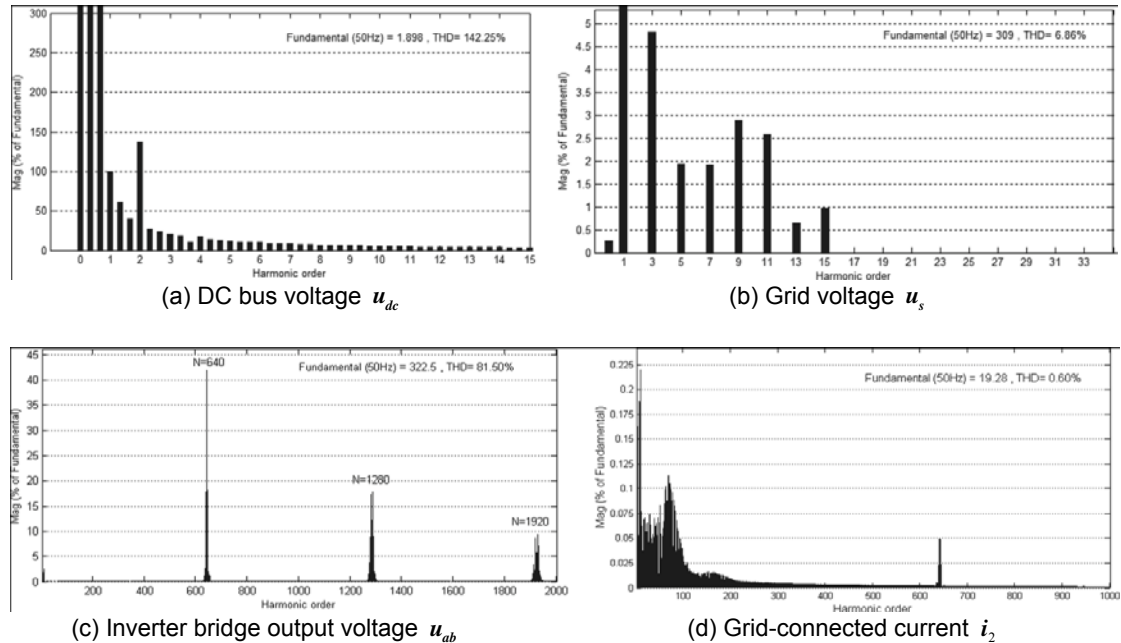


Figure 9. Harmonics Spectrum

Figure 8 reveals the waveform of the grid-connected current when the 3kW inverter experiment system operates stably adopting the combined control scheme proposed in this paper. In Figure 9(a), the DC bus voltage includes low-order harmonics (mainly the second component) with fairly small amplitude. As shown in Figure 9(b), there are numerous low-frequency harmonics (mainly the odd-order components) in the grid voltage. It can be found out in Figure 9(c) that the output voltage of the inverter bridge contains a small number of low-frequency harmonics and a large number of high-frequency harmonics (near the frequency that is as even times as the switching frequency). In Figure 9(d), the THD of the grid-connected current is only 0.60%, because the high-frequency harmonics have been filtered effectively, and furthermore, the low-order harmonics have been dramatically suppressed by the combined control scheme.

## 6. Conclusion

In this paper, the harmonic components of grid-connected current are systemically and quantitatively analyzed, including the high-frequency harmonics caused by the modulation, and the low-frequency harmonics injected by the inherent non-linear characteristics and dead-time effects of switching tubes along with the DC voltage secondary pulsation and the grid disturbance. As a result, the generation power, power factor and harmonic distortion of the grid-connected inverter are tremendously affected.

State feedback can suppress resonance peak, improve the stability and the rapid response capability of the system. Through the DC voltage feedforward, the gain of the inverter bridge can be stabilized, as well as the impact of DC voltage fluctuations can be decoupled. Similarly, the impact of the grid harmonic pollution upon grid-tied current can be compensated

by inserting the grid voltage feedforward. The embedded repetitive controller can effectively damp the low-order harmonics injected by periodical disturbances, thus it can increase the system steady-state accuracy and achieve a good instruction dynamic tracking performance. The harmonic distribution of experimental voltage and current is in line with the harmonic analysis discussed in this paper. The THD of the grid-tied current is rather small and the quality of the waveform is quite good, which verify the validity of the presented combined control scheme.

### Acknowledgement

This work was supported by the National golden sun demonstration project (Grant Nos. 20090718047), and the Chinese Universities Scientific Fund (Grant Nos. CUSF-DH-D-2013055).

### References

- [1] R Teodorescu, M Liserre, P Rodriguez. *Grid Converters for Photovoltaic and Wind Power Systems* Hoboken, NJ: Wiley. 2010.
- [2] Lele Peng, Yize Sun, Zhuo Meng. A new method for determining the characteristics of solar cells [J]. *Journal of power sources*. 2013; 227: 131-136.
- [3] F Blaabjerg, R Teodorescu, M Liserre. Overview of control and grid synchronization for distributed power generation systems. *IEEE Trans. Power Electron.*, 2006; 53(5): 1398–1409.
- [4] Wang Pan, Liu Fei, Zha Xiaoming. Research on a New Type of Energy Feedback Cascade Multilevel Inverter System. *TELKOMNIKA Indonesian Journal of Electrical Engineering*. 2013; 11(1): 494–502.
- [5] B Bolsens, K De, J Van, J Driesen, R Belmans. Model-based generation of low distortion currents in grid-coupled PWM-inverters using an LCL output filter. *IEEE Trans. Power Electron.*, 2006; 21(4): 1032–1040.
- [6] M Liserre, F Blaabjerg, S Hansen. Design and control of an LCL-filter based three-phase active rectifier. *IEEE Trans. Ind. Appl.*, 2005; 41(5): 1281–1291.
- [7] TCY Wang, ZH Ye, G Sinha, XM Yuan. *Output filter design for a grid-interconnected three-phase inverter*. Proc. IEEE PESC. 2003: 779–784.
- [8] Huang Wangjun, Zeng Zhigang, Zhou Huifang. Modeling and Experimental Study on Grid-Connected Inverter for Direct Drive Wind Turbine. *TELKOMNIKA Indonesian Journal of Electrical Engineering*. 2013; 11(4): 2064-2072.
- [9] Y Sozer, DA Torrey. Modeling and control of utility interactive inverters. *IEEE Trans. Power Electron.*, 2009; 24(11): 2475–2483.
- [10] Eric Wu, Peter W Lehn. Digital Current Control of a Voltage Source Converter with Active Damping of LCL Resonance. *IEEE Trans. Power Electron.*, 2006; 21(5): 1364–1373.
- [11] Timbus, M Liserre, R Teodorescu, P Rodriguez, F Blaabjerg. Evaluation of current controller for distributed power generation systems. *IEEE Trans. Power Electron.*, 2009; 24(3): 654–664.
- [12] M Castilla, J Miret, J Matas. Control design guidelines for single-phase grid-connected photovoltaic inverters with damped resonant harmonic compensators. *IEEE Trans. Industrial Electron.*, 2009; 56(11): 4492–4501.
- [13] PT Cheng, JM Chen, CL Ni. Design of a state-feedback controller for series voltage-sag compensators. *IEEE Trans. Ind. Appl.*, 2009; 45(1): 260–267.
- [14] P Mattavelli, FP Marafão. Repetitive-Based Control for Selective Harmonic Compensation in Active Power Filters. *IEEE Trans. Industrial Electronics*. 2004; 51(5): 1018–1024.
- [15] IEEE Std.929-2000. IEEE Recommended Practice for Utility Interface of Photovoltaic (PV) Systems.